This Publication Is Distributed To Members Only

Harmonics and Transients Tech Notes

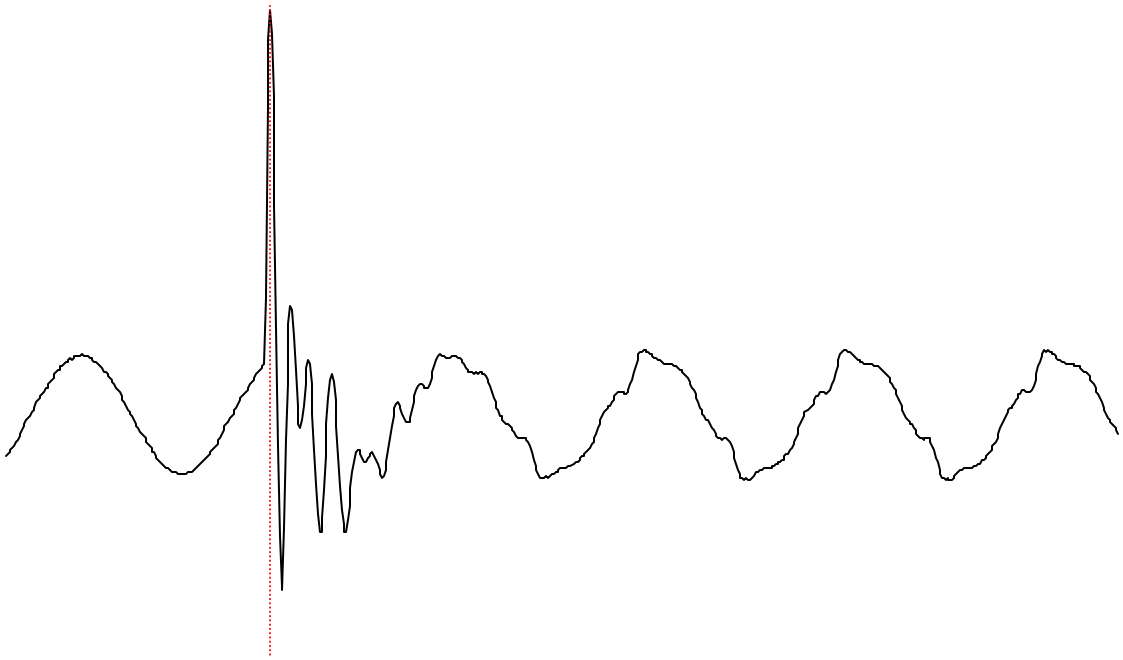

Issue # 00-1 ***February 2000*** ***Editor: Karen Brown***

Project Manager: Tom Grebe

In this issue:

Letter from the Editor I
Effect of Inductance on Motor-Side Harmonics 1
Power Quality Impact on Thermal Behavior and Life Expectancy of Three-Phase Induction Motors…9
A Method for Characterization of Three-Phase Unbalanced Dips from Recorded Voltage……
Waveshapes 25

Letter from the Editor:

Dear PATH Members:

You will note that there has been a change in the PATH User Group staff. Sandy Smith has accepted the position of regional marketing director with Bluestar of Memphis, Tennessee. We here at Electrotek wish him much success in his new position. With Sandy's departure I will be executing the duties of editor for the PATH User Group. If you have questions or concerns involving the newsletter or tech notes, please do not hesitate to contact me.

Karen Brown, Technical Coordinator
Phone: 865.470.9222 ext. 143
Fax: 865.470.9233
E-mail: karenb@electrotek.com

We would like to welcome you to another edition of *Tech Notes*. We hope you find this issue to be both informative and interesting. This issue features

- HarmFlo analysis of harmonics generated by a converter
- Thermal behavior analysis of three-phase induction motors under non-ideal conditions
- Proposal for characterization of voltage dips as experienced by three-phase load

Sincerely,

Karen Brown
Technical Coordinator
Editor, PATH Users Group / PQView User Group

EFFECT OF INDUCTANCE ON MOTOR-SIDE HARMONICS

Bruno Osorno
California State University Northridge
Department of Electrical and Computer Engineering
Northridge, CA

Abstract: Motor side harmonics depend on the design of the converter. This paper will discuss the analysis of harmonics generated by a converter using HarmFlo.

Introduction

Speed drive manufacturers look mostly at the harmonics produced on the motor's side, consequently the converter's harmonics are the ones to observe. Since the voltage waveform depends on the impedance of the motor, the waveform is directly dependent on the harmonic frequencies. Six step converters can reach up to 40% current distortion with the additional I^2 R heating. Therefore, motors used under these circumstances must be designed to withstand the extra heating. This extra loss of energy can be reduced if we decrease the harmonic content of the current going into the motor.

Diagrams

DIAGRAMS: The first step was to produce a simple one-line diagram. The components are an ac three-phase source connected to a step down transformer and the secondary of the transformer is connected to a drive ASD (adjustable speed drive). See Figure 1.

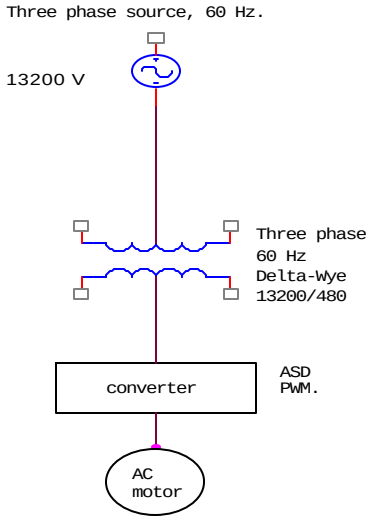

Figure 1: One Line Diagram of a Simple ASD

The ASD is composed of a rectifier and an inverter. The rectifier dc output is inverted through a voltage source inverter (VSI). A typical circuit is shown in Figure 2 [1]. The ac motor is usually a squirrel cage induction motor. A synchronous motor can be used for more precise speed regulation. The control of the speed is done through controlling the frequency of the current and voltage signal output.

The introduction of an inductor (choke) reduces dramatically the distortion of the signal (current) [3]. This was furthermore proved in our HarmFlo simulation by introducing a branch with inductance between the transformer and the ASD.

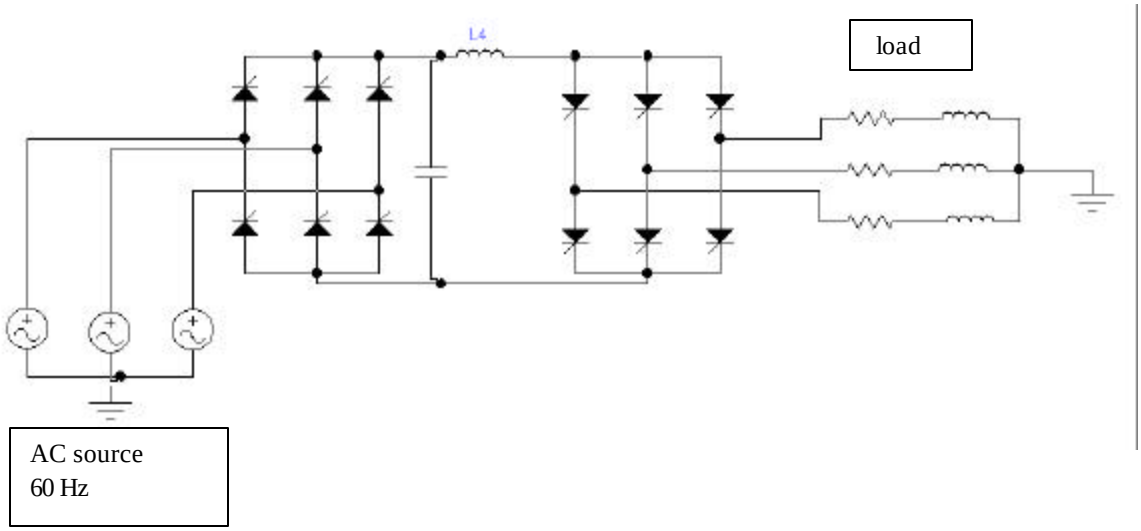

Figure 2: Typical ASD Circuit

Simulation

The theory of these converters is covered in most textbooks in power electronics [1], [4], [5]. So we will focus in the simulation using HarmFlo and how by using a simple inductor connected to the converter's input, reduces the harmonic content. Of course this inductor acts as a filter, but also it shows that the reactance added to this converter helps control the level of harmonic distortion [3]. Correlating this addition of reactance, it may help the designers of induction motors realize that the application of induction motors in ASD requires a closer look into the impedance that the converter sees.

Figure 3 shows the spectrum of current output without branch addition. It can be observed (apparent observation) that all the values of the output are higher than the one for the output current with the branch included. See Figure 4.
Figure 3 shows the spectrum of current output without branch addition for the both cases, without and with branch reactance. Again, the same comment applies for the spectrum.

The simulation attempted in this paper was done for only one case of the firing angle, it is quite difficult to do the firing angle range of simulation under this circumstances (parametric solution). That is, the harmonic values of distortion for the converter must be input for the simulation to run. In which case once we have the harmonic values of the converter we can input them into the program and then look for a method for the decrease of harmonic levels and consequently conform to IEEE standards. In the future it would be good to get the range of harmonic distortion over a range of firing angle values from the manufacturers, and then run HarmFlo and attempt to obtain an output. This output could be analyzed to see under what values of load the ASD does not meet IEEE standards.

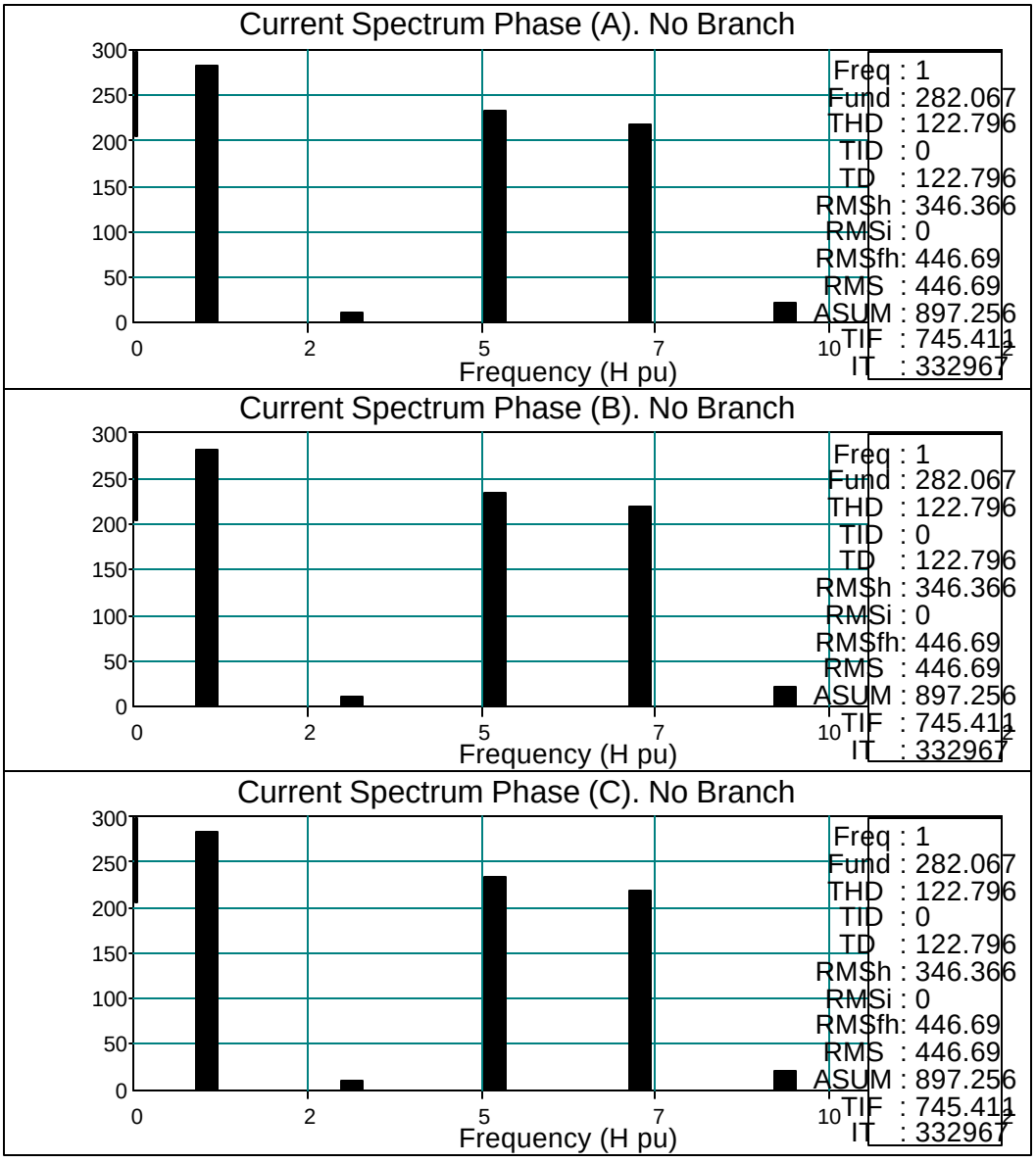

Figure 3: Spectrum of Current Output without Branch Addition

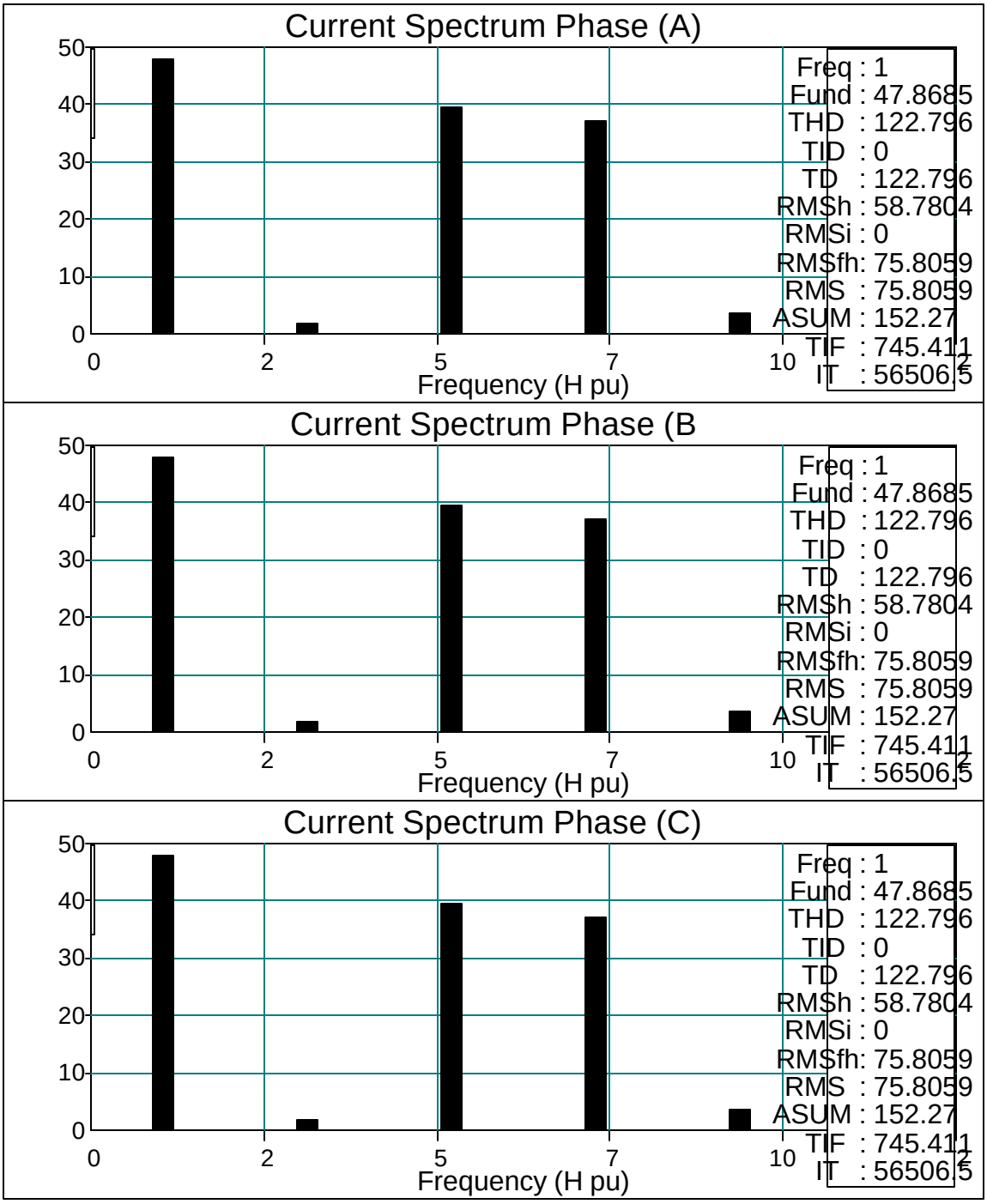

Figure 4: Spectrum of Current Output with Branch Addition

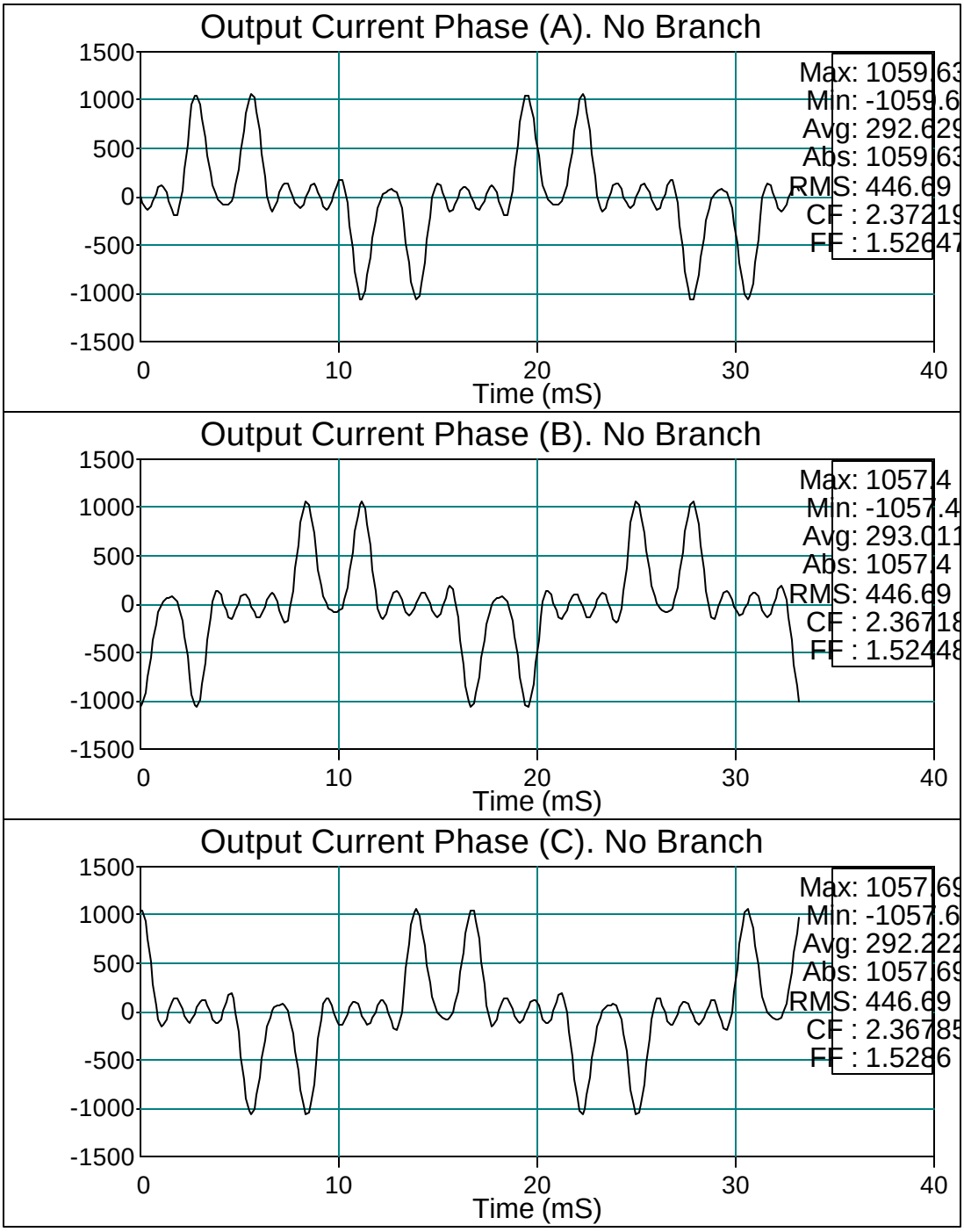

Figure 5: Time Domain Current Output without Branch Addition

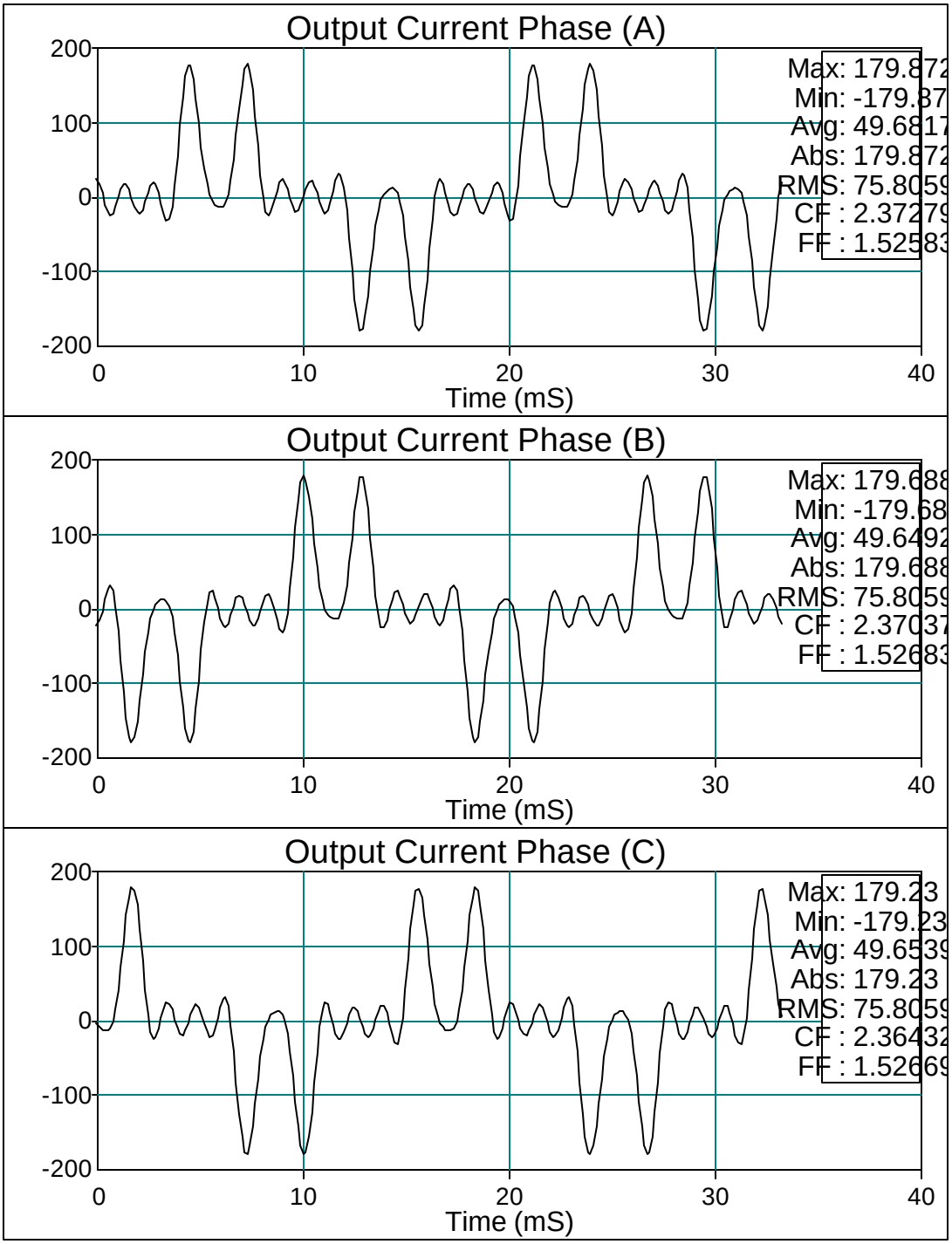

Figure 6: Time Domain Current Output with Branch Addition

Conclusions

According to Pace [3] inductors will have the effect of harmonic reduction if they are placed at the input of the converter. This is not new, what is exciting is the program HarmFlo that allows to run thus simulations with the minimum amount of effort, and automatically give us the IEEE 519 standard compliance. The output processor "TOP" is perhaps the most powerful tool of the program. For example from both outputs done in this paper we could have readily developed the following table for comparison purposes.

Table 1: Effect of Inductance on Fundamental Current

	Phase A. No Branch	Phase A.
Fund	282.0	47.86
THD	122.796	122.79
TD	122.796	122.79
TIF	745.4	745.4
IT	332967	56506.5

From the table above we can see the effect of the inductance on the fundamental current. The change is of around 600% and the IT also had a dramatic change. THD remain the same because the inductor had no effect on the wave-shape of the current.

References

[1] C. Dugan, et al. "Electric Power Systems Quality." McGraw-Hill, 1999.

[2] N. Mohan, et al. "Power Electronics." Wiley, second edition. 1995.

[3] D. Pace. "Power Electronic Converter Harmonics." IEEE press, 1996.

[4] A. Trzynadlowski. "Modern Power Electronics." Wiley, 1998.

[5] M. Rashid. "Spice for Power Electronics and Electric Power." Prentice-Hall, 1993.

[6] IEEE 519 Recommended Practices and Requirements for Harmonic Control in Electrical Power Systems.

POWER QUALITY IMPACT ON THERMAL BEHAVIOR AND LIFE EXPECTANCY OF THREE-PHASE INDUCTION MOTORS

Olívio C. N. Souto (MSc) José C. de Oliveira (PhD) Luciano M. Neto, Dr
Electrical Engineering Department
Federal University of Uberlandia

Abstract: This paper deals with thermal behavior analysis of three-phase induction motors under non-ideal supply conditions. The motors are of squirrel cage type and the non-ideal conditions are associated to harmonics, unbalances, voltage sag and swell, etc. The studies are carried out using a comprehensive methodology that handles electrical, mechanical and thermal models in a simultaneous way. The approach is then implemented into a time domain program known as SABER simulator. Computational studies are then performed to evaluate motor temperature rise and life reduction under non-ideal conditions.
***Index terms*--Induction Motors, Harmonics, Power Quality, Simulation, Thermal design**

Introduction

Electric power quality has captured considerable attention from utility companies as well as their customers. The major reasons for the growing concerns are the continued proliferation of sensitive equipment and the increasing application of power electronic devices resulting in power supply degradation. In addition, customers have become less tolerant to power quality disturbances. In relation to this subject, many studies, researches and developments have been reported in order to evaluate, assure and even to improve the quality of electric power systems [1][2].

Focusing on the interaction between voltage quality and the supplied load, it must be noticed that, in a typical industry load composition, about 80 % of the electric consumption comprises three-phase induction motors. Therefore, any power quality study, as well as any energy saving investigation procedure should not disregard induction motor performance under loss of quality conditions. Although the effects of harmonic voltage distortion on induction motor behavior and loss of life have been widely analyzed [3,4], the power quality context includes other non-ideal conditions than harmonic distortion. So, problems such as voltage unbalance, voltage variations, transients, etc, should be necessarily included.

The induction motor voltage supply loss of quality usually results in an augment of internal heat generation [5]. The consequence is an increase of stator and rotor temperature that may result in thermal failure and machine loss of life. Thus, to guaranty the specified motor lifetime, winding temperature must remain below the insulation temperature class limit [6]. In relation to the determination of induction motor temperature it is possible to use direct and indirect methods. The first involves sensors to measure the internal temperature and the second approach utilizes thermal models [7][8].

Focusing the relationship between supply quality conditions and motor thermal performance, this paper discusses the investigation of thermal operating conditions associated with the squirrel-cage three-phase induction motor under non-ideal voltage conditions. Using a time domain method, electrical, mechanical and thermal induction motor models are proposed to handle the

overall effects in a simultaneous way. By evaluating motor final temperature, it is then possible to estimate the effect of voltage quality degradation upon the machine life expectancy. A comprehensive computer program is then obtained using a commercial simulator known as SABER and studies are carried out to illustrate the overall motor losses, temperature and life expectancy under power quality deterioration.

Electromechanical Model

The model implemented is the three-phase independent ABC reference frame to represent the squirrel-cage induction motor. This approach provides a flexible and versatile way to investigate machine performance.

A. Electric Equation

According to [9], by defining the stator phases as "abc" and rotor phases as "ABC", the instantaneous voltage is given in the ABC reference frame by expressions such as:

$$v_i = r_i\, i_i + \frac{d\,\lambda_i}{d\,t} \tag{1}$$

where:

- v_i - phase i instantaneous voltage
- r_i - motor winding resistance
- i_i - phase i instantaneous current
- λ_i - phase i coil flux

The subscript " i " can be made equal to "a, b, c, A, B and C", to denote stator and rotor quantities, respectively.

B. Mechanical Equation

The mechanical equations are then coupled to the electric system via the electromagnetic torque. It can be done on the basis of energy flow through the machine. This yields to:

$$T = \frac{p}{2} \sum_i \sum_j i_i\, j_j \frac{d\,L_{ij}}{d\theta_R} \tag{2}$$

with:

- i_i - stator phase current (i = "a, b, c")
- i_j - rotor phase current (j = "A, B, C")
- p - machine number of poles
- L_{ij} - inductance matrix
- θ_R - rotor mechanical angle

C. Electromechanical Dynamic Equations

The full set of differential equations necessary to represent the overall motor electromechanical system can then be written using the previous equations. The instantaneous general electric equation using ABC reference frame is then:

$$\frac{d[I]}{dt} = [L]^{-1}\left([V] - [D][I]\right) \tag{3}$$

The mechanical equations to describe the load and motor coupling can be given by:

$$\frac{d\omega_R}{dt} = \frac{p}{J}\left(T - T_c\right) \tag{4}$$

$$\frac{d\theta_R}{dt} = \omega_R \tag{5}$$

where:

- [V] - stator and rotor voltage vector
- [I] - stator and rotor current vector
- [L] - winding inductance matrix
- [D] - d [L]/dt + [R] matrix
- [R] - stator and rotor winding resistance matrix
- ω_R - rotor shaft speed
- J - motor inertia moment
- T - electromagnetic torque given by (2)
- T_c - load torque

The inductance matrix and the torque equation can be expressed as follows:

$$[L] = \begin{bmatrix} L_{SS}+L_S & M_{SS} & M_{SS} & MA_{SR} & MB_{SR} & MC_{SR} \\ M_{SS} & L_{SS}+L_S & M_{SS} & MC_{SR} & MA_{SR} & MB_{SR} \\ M_{SS} & M_{SS} & L_{SS}+L_S & MB_{SR} & MC_{SR} & MA_{SR} \\ MA_{SR} & MC_{SR} & MB_{SR} & L_{RR}+L_R & M_{RR} & M_{RR} \\ MB_{SR} & MA_{SR} & MC_{SR} & M_{RR} & L_{RR}+L_R & M_{RR} \\ MC_{SR} & MB_{SR} & MA_{SR} & M_{RR} & M_{RR} & L_{RR}+L_R \end{bmatrix} \tag{6}$$

$$T = -L_{SR}\frac{p}{2}\left\{\begin{array}{c} \left(i_a i_A + i_b i_B + i_c i_C\right)\operatorname{sen}\left(\theta_R\right) \\ +\left(i_a i_B + i_b i_C + i_c i_A\right)\operatorname{sen}\left(\theta_R + \frac{2\pi}{3}\right) \\ +\left(i_a i_C + i_b i_A + i_c i_B\right)\operatorname{sen}\left(\theta_R - \frac{2\pi}{3}\right) \end{array}\right\} \tag{7}$$

where:

$$MA_{SR} = L_{SR}\cos\left(\theta_R\right) \tag{8}$$

$$MB_{SR} = L_{SR} \cos\left(\theta_R + \frac{2\pi}{3}\right) \quad (9)$$

$$MC_{SR} = L_{SR} \cos\left(\theta_R - \frac{2\pi}{3}\right) \quad (10)$$

In the above equations:

L_S	- stator leakage inductance
L_R	- rotor leakage inductance
$L_{SS} = L_{RR} = L_{SR}$	- 2/3 of the magnetising inductance
M_{SS}	- stator mutual winding inductance
M_{RR}	- rotor mutual winding inductance
MA_{SR}	- phase A stator to rotor mutual inductance
MB_{SR}	- phase B stator to rotor mutual inductance
MC_{SR}	- phase C stator to rotor mutual inductance

Thermal Model

To investigate the induction motor temperature rise with loss of power supply quality, a three-phase thermal model is proposed in this paper. It represents both the stator and rotor equivalent parameters in terms of lumped elements. No thermal coupling between rotor and stator is considered in the model. It has been found that the air gap provides a barrier to heat transfer from stator to rotor and vice-versa [10]. Therefore, the model utilizes lumped parameters such as: thermal conductances or resistances, thermal storage capacitor and heat sources. These are given in Figure 1a and 1b.

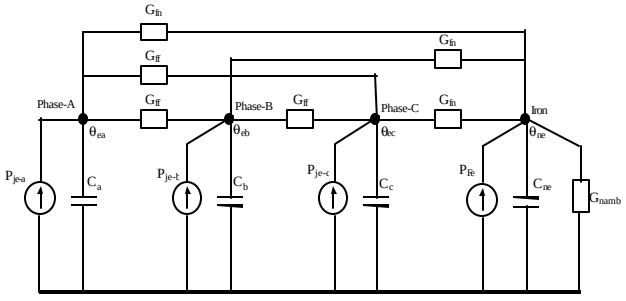

Figure 1a: Stator Thermal Model

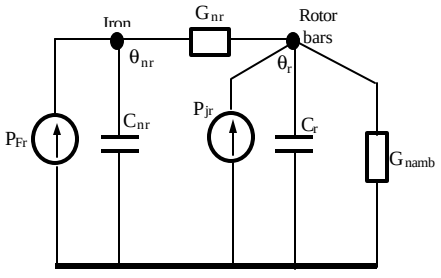

Figure 1b: Rotor Thermal Model

In the above figures:

- P_j - Subscripted by a complementary identification represents the heat sources;
- G - Followed by a corresponding subscript means the thermal conductance between two different surfaces within the motor;
- C - The same as above for thermal capacitance;
- θ - Temperature at a given location.

The above-proposed model is a simple and efficient way of dealing with the motor thermal performance without going into deep heat flow theory. Besides, the necessary parameters do not need detailed design information, but they can be derived from ordinary motor data and manufacturer information. According to the equivalent circuit shown in Figure 1a and 1b, the model allows for steady state and transient temperature rise in the machine. It must be pointed out that temperature rise refers to the conductor temperature in relation to the ambient air temperature. In this paper, the ambient temperature in the vicinity of the motor was taken as 40 ^{o}C.

A. Thermal Conductances

From traditional theory, an equivalent thermal resistance or conductance defines the heat transfer capability between two different surfaces with distinct temperatures. To evaluate the thermal resistances or conductances shown in the equivalent circuit, it is necessary to know only the motor rated losses and the insulation maximum temperature rise allowable. The insulation class defines this. The calculation utilizes normal conditions for the supply and motor operation. Some authors use the induction motor dimensions and physical information to calculate these thermal parameter, however, this is a very hard task [8]. In this paper, the induction motor used has a class B isolation, thus, the hot spot permitted conductor temperature is 130 ^{o}C [6]. The stator winding to iron thermal conductances are then determined considering the above temperature and the rated conductor losses. Following the same procedure, the motor iron to external surface conductance is obtained taking into account the motor ventilation [14]. Another thermal conductance shown in Figure 1a expresses the phase-to-phase thermal conductance. This is of major importance when the motor is running under unbalanced supply voltage conditions. In this case, it is possible to have heat flow between phases. Reporting to [10], these parameters are approximately twice the phase to iron thermal conductance.

B. Thermal Capacitance

The concept of thermal resistance is associated to the amount of heat transference between two different areas under distinct temperatures. On the other hand, there is a complementary effect to be considered. This is the heat storage capacity related to any physical body. The so-called thermal capacitance is used to express this capacity. Besides providing the heat storage, this parameter allows for the inclusion of the time delay to change any temperature at given surface spot. This capacitance can be calculated from machine physical data [7]. In a general way, the final equation is given by expression (11).

$$C = m\,c \quad [Ws/^{o}C] \tag{11}$$

where:

- c - isolation specific heat [Ws/ ^{o}C kg]
- m - winding mass [kg]

C. Motor Losses Distribution

The internal heat sources are composed by copper, iron, stray and mechanical losses. The copper losses (stator and rotor) are calculated using the following equation:

$$P_j = R\, i(t)^2 \quad [W] \tag{12}$$

where:

P_j -copper losses [W]
R -stator or rotor resistance [ohm]
i (t) -conductor current [A]

It must be emphasized that there is a non-linear relationship between rotor impedance and frequency (skin effect). This phenomenon occurs mainly at the rotor bars and it has been implemented into the time domain program according to procedures given in [13][14]. The stator resistance was kept constant. Another important effect is related to the copper losses dependence with conductor temperature. This was also considered by adjusting the stator and rotor winding resistance for each time step.

The additional stray load losses are relatively small and they can be taken to be a small proportion of the rated input electrical power. A typical value of 0.5 % was considered [6]. The iron losses are obtained using the equivalent resistance. This parameter can be directly derived from induction motor test and it includes stator and rotor losses. Although this effect is evenly distributed between stator and rotor, it must be recognized that the largest component is concentrated in the stator. A resistant torque included into the shaft load represents the mechanical losses.

D. General Thermal Equation

The thermal model can be finally described by a set of four heat equations (one for each node). The general mathematical expressions to represent the relationship between stator heating and temperature are given bellow.

$$\frac{d[\theta]}{dt} = [C]^{-1}\left([P] - [G][\theta]\right) \tag{13}$$

where:

[θ] - temperature rise matrix;
[C] - thermal capacitance matrix;
[P] - motor losses vector;
[G] - thermal conductance matrix.

The stator thermal capacitance and conductance matrixes are given by:

$$[C]=\begin{bmatrix} Ca & 0 & 0 & 0 \\ 0 & Cb & 0 & 0 \\ 0 & 0 & Cc & 0 \\ 0 & 0 & 0 & Cne \end{bmatrix} \tag{14}$$

$$[G]=\begin{bmatrix} 2Gff+Gfn & -Gff & -Gff & -Gff \\ -Gff & 2Gff+Gfn & -Gff & -Gff \\ -Gff & -Gff & 2Gff+Gfn & -Gff \\ -Gfn & -Gfn & -Gfn & 3Gfn+Gna \end{bmatrix} \tag{15}$$

where:

Ca, Cb, Cc	- stator winding thermal capacitances;
Cne	- stator iron thermal capacitance;
Gff	- phase to phase stator thermal conductance;
Gfn	- phase to iron stator thermal conductance;
Gna	- iron to ambient thermal conductance.

A similar set of equations can be obtained to describe the thermal relationship between rotor heating and temperature. However, these have been omitted. They can be found in Ref. [13].

Life Expectancy Estimation

In accordance with [12], the thermal degradation of organic and inorganic material of an electric device is mainly caused by temperature rise beyond the rated value. This loss of useful life can be estimated by the reaction rate equation known as the Arrhenius expression:

$$\frac{d\rho}{dt} = A\, e^{-\frac{E}{k\theta}} \tag{16}$$

where:

$d\rho/dt$	- lifetime expectancy reduction in isolation properties
A	- constant related to the type of material
k	- Boltzmann constant
θ	- absolute temperature in Kelvin
E	- activation energy of the aging reaction

To establish a comparison between the motor life expectancy under ideal and non-ideal conditions, by applying equation (16), it is possible to verify the relationship between motor loss of life and temperature rise [3].

$$\rho_1 = \rho_2 . e^{-\left(\frac{E}{k}\right)\frac{\Delta\theta}{\theta_2 \cdot (\theta_2+\Delta\theta)}} \tag{17}$$

where:

ρ_1 - new motor lifetime expectancy;
ρ_2 - rated motor lifetime expectancy;
E - activation energy;
k - Boltzmann constant;
$\Delta\theta$ - temperature rise in relation to θ_2 in ^oC;
θ_2 - rated temperature in Kelvin.

Computational Results

In order to investigate the induction motor thermal behavior under voltage supply conditions with power quality loss, different computer simulations were carried out using both ideal and non-ideal voltage conditions. The results obtained are related to stator winding, stator iron and rotor winding temperature. It is assumed that the power quality degradation was caused by voltage unbalance and distortion. The three-phase squirrel-cage induction motors parameters are given in Table I. For simulation purposes, the motor mechanical load was taken as 100 %.

Table I: Motor Parameters

PARAMETERS	UNIT	VALUE
Rated Power	*Hp*	3
Rated Voltage	*V*	220
Winding connection	-	Delta
Rated Speed	*rpm*	1730
Stator resistance - R_s	*ohm*	2.31
Rotor resistance - R_r	*ohm*	2.6191
Stator reactance - X_s	*ohm*	3.5336
Rotor reactance - X_r	*ohm*	2.3675
Magnetising reactance - X_m	*ohm*	87.9959
Iron losses resistance - R_m	*ohm*	2008.02
Inertia moment - j_m	$Kg.m^2$	0.0075
Number of poles - np	-	4

Table II summarizes the different situations related to the supply power quality degradation used for study purposes.

Table II: Cases Studied

CASE	CHARACTERISTICS
Case 1	Motor supplied with a purely sinusoidal, symmetric and balance voltage.
Case 2	Voltage supply with 5% of unbalance.
Case 3	Voltage supply with 20% of harmonic distortion.
Case 4	Voltage supply with 5% of unbalance and 22% of harmonic distortion.

A.. CASE 1 – Ideal Supply

This first situation gives the motor thermal and electrical operation results under ideal conditions. The thermal quantities are the stator winding and rotor temperatures. Figure 2a and 2b illustrate

the voltage supply and the motor line A current. Part of the motor transient starting current can be seen.

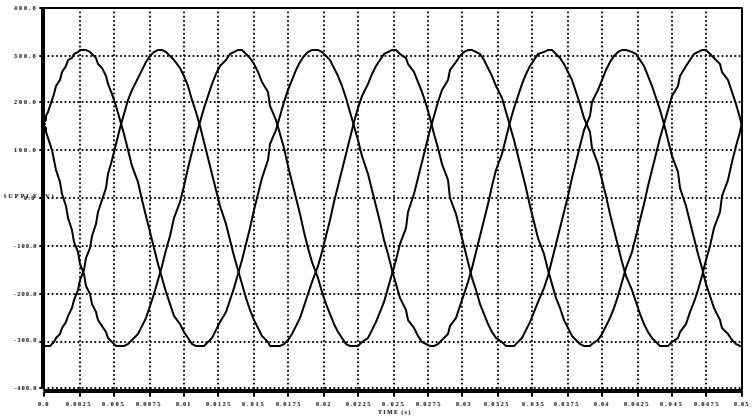

Figure 2a: Steady State Voltage Supply

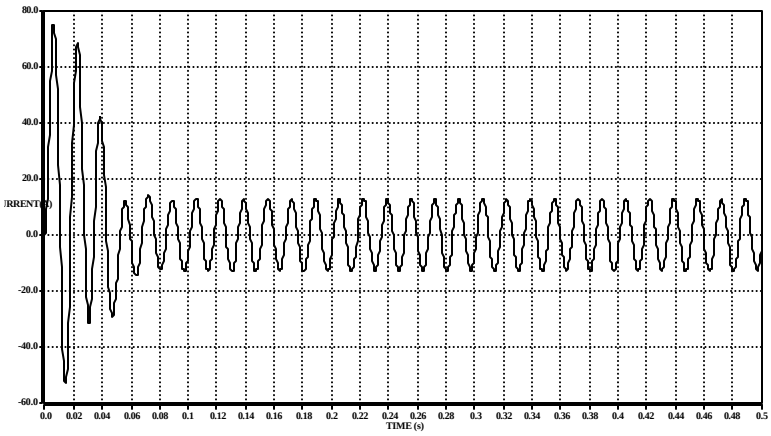

Figure 2b: Phase A Line Current

The motor transient and steady state thermal results shown in Figure 3a and 3b express the temperature at stator and rotor windings. The steady state stator winding temperature achieved 122 ^{o}C and the rotor 185 ^{o}C.

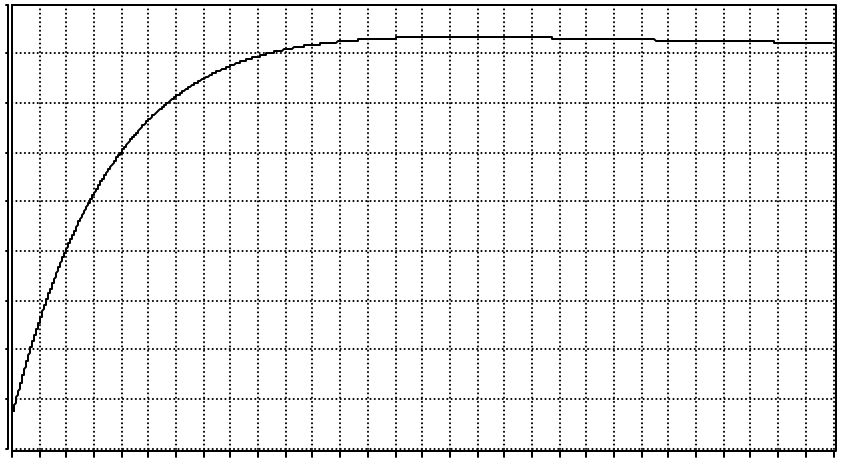

Figure 3a: Stator Winding Temperature

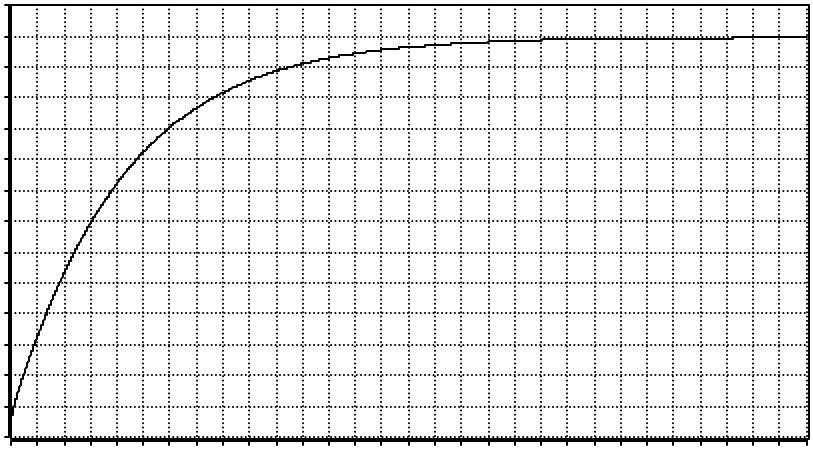

Figure 3b: Rotor Winding Temperature

B. CASE 2 – Supply with 5% of Voltage Unbalance

The presence of voltage unbalance in any industrial power system complex is always certain. This item of power quality degradation is a well-known subject and the corresponding effects are well established. By assuming the degree of asymmetry as being 5%, the investigations were carried out to illustrate the induction motor thermal performance. This problem is aggravated by the fact that the presence of a small unbalance in the voltage supply causes a larger unbalance in the line currents.

The stator winding temperature under a balanced sinusoidal and unbalanced supply conditions are comparatively shown in Figure 4. The new steady state temperature reached 128 ^{o}C.

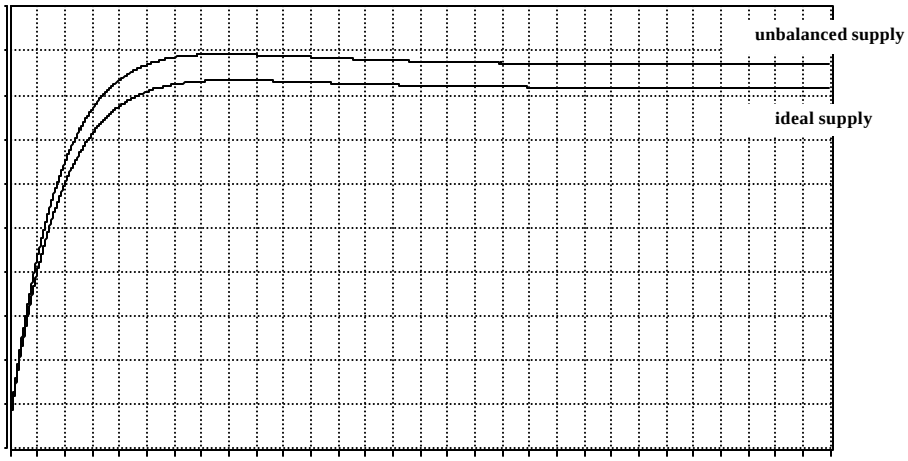

Figure 4: Stator Winding Temperature under Ideal and Unbalanced Supply

C. CASE 3 Supply with 22% of Harmonic Distortion

The loss of quality investigated in this case is related to harmonic distortion superimposed on the fundamental voltage supply. The strategy is to maintain the fundamental voltage magnitude and to add 5, 7, 11 and 13 harmonic orders to produce a total harmonic distortion (THD_V) of 22 %. Figure 5a and 5b illustrate, respectively, the distorted voltage supply and stator winding temperature.

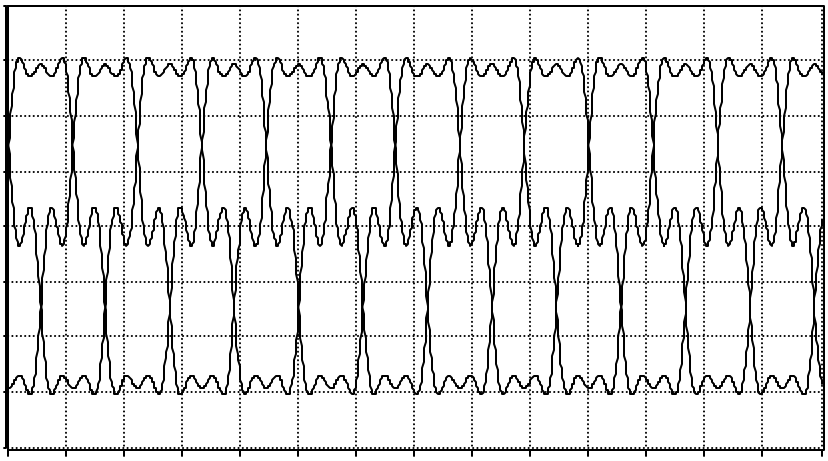

Figure 5a: Three-Phase Line Voltage

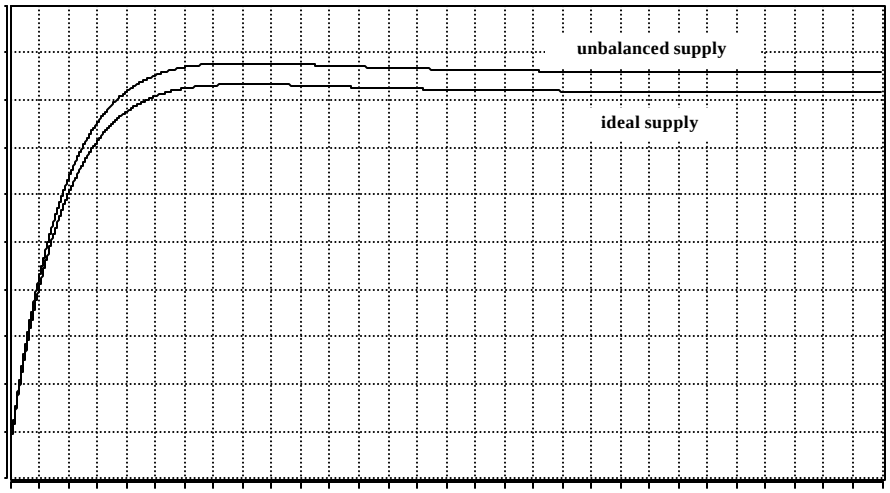

Figure 5b: Stator Winding Temperature

Although the temperature results for both sinusoidal and distorted conditions are quite close, it can be noticed that the harmonic distortion led to a final temperature of 125.9 ^{o} C. This corresponds to an increase of 3.9 ^{o} C in relation to the ideal case.

D. CASE 4 –Supply with 30% of Harmonic Distortion and 3% of Voltage Unbalance

This final study aims to investigate the induction motor behavior when the voltage supply shows a degradation associated to harmonic distortion and voltage unbalance in a simultaneous way. Although this could be considered quite a rare operational condition, the situation is not absolutely theoretical. Besides, when one considers the case of induction motor application supplied by frequency converters, the above disturbances can be closer to real conditions. Figure 6a shows the line current and Figure 6b the stator winding temperature. The stator temperature rise is substantially high to cause motor overheating and reduction of life expectancy.

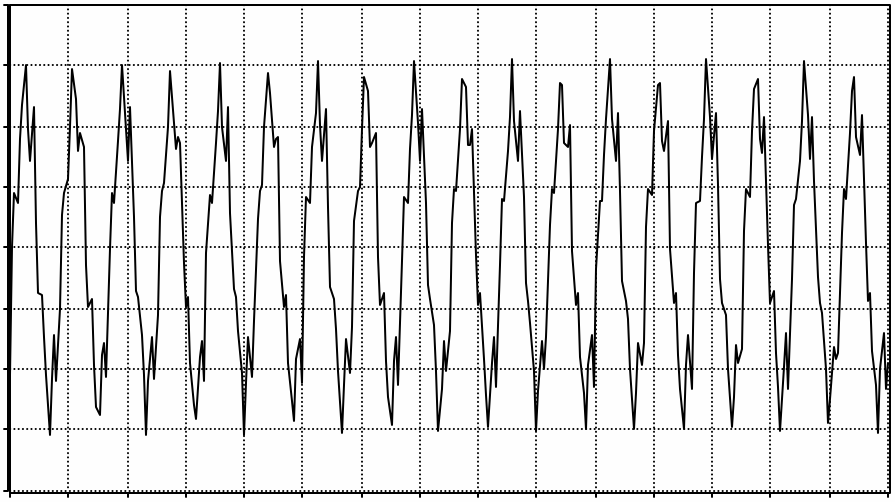

Figure 6a: Line Current

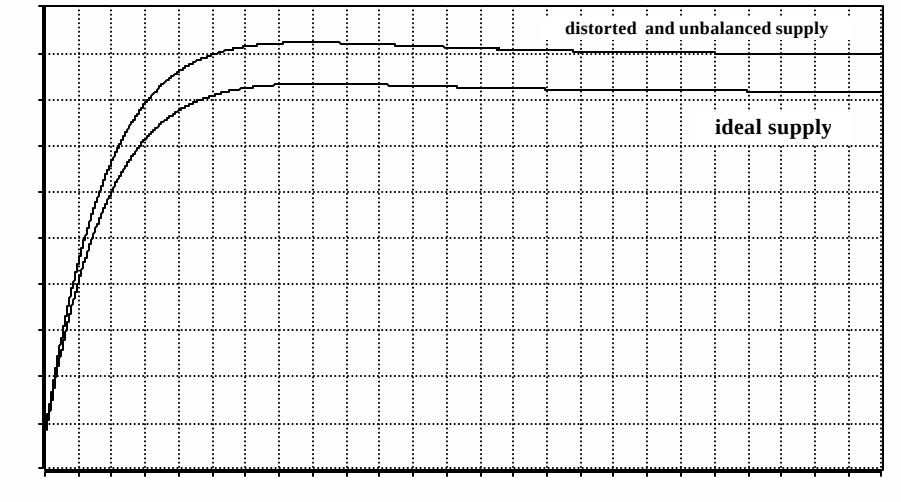

Figure 6b: Stator Winding Temperature

Life Expectancy Estimation

Several other simulations using different levels for the disturbance items were then performed to investigate the induction motor thermal behavior in a more comprehensive way. The steady state stator winding temperature and the corresponding life reduction under different level of unbalances and distortions are illustrated in Table III. By applying equation (19), it is possible to calculate the corresponding motor life expectancy reduction. The final results are clear enough to emphasize the strong relationship between temperature and motor useful life.

Table III: Relationship Between Disturbances and Life Expectancy

	Unbalance				Harmonic				
	2	5	10	15	5	10	15	20	25
Stator winding temperature [°C]	**122.7**	**127.0**	141, 0	**161.2**	**123.4**	**123.5**	**123.7**	**125.9**	**126.8**
Life expectancy reduction [%]	**4**	**32.9**	**80.14**	**97**	**9.15**	**9.89**	**11.8**	**26.9**	**31.6**

Conclusions

This paper focused on the behavior of induction motors under different and simultaneous power quality loss conditions. For a comprehensive way of dealing with supply degradation, motor electrical and thermal equations were proposed. The approach uses basic electrical and thermal concepts applied to quantify motor operating temperature and life expectancy. The necessary data to feed the equations can be derived from classical manufacturer information. The models

were implemented into a time domain simulator known as SABER software. The program obtained can cope with different and simultaneous items of power degradation and the motor was modeled using an independent three-phase representation. Both transient and steady state electrical and thermal behavior concerning the motor operation can then be predicted. Using the program, a set of non-ideal operating conditions was established and computational studies were carried out. The results were clear enough to illustrate the effect of power quality upon motor performance and life expectancy. In accordance with the results, under poor supply conditions, in order to avoid motor damage or to keep the useful life, it is necessary to de-rate the motor. Although only harmonic distortion and voltage unbalance were considered for the studies, the authors would like to state that any other non-ideal condition might be easily handled. In addition, the authors are working towards laboratory validation to verify the proposed model accuracy.

References

[1] Dugan, R. et al. *Electrical Power System Quality*, McGraw-Hill, USA, 1996.

[2] Arrilaga, J. et al. *Power Systems Harmonics*, John Wiley & Sons, USA, 1985.

[3] E. F. Fuchs, D. J. Roesler and F. S. Alashhab. "Sensitivity of Electrical Appliances to Harmonics and Fractional Harmonics of the Power Systems Voltage" *Part I: Transformers and Induction Machines, IEEE Power Delivery*, Vol. PWRD-2, No. 2, April 1987.

[4] A. E. Emanuel. "The Effect of Harmonic Randomness upon Temperature Rise of Electrical Equipment", *Proceedings of International Conferences on Harmonics in Power Systems, ICHIPS III*, Nashville, Indiana, October 1988, pp. 257-62.

[5] J. T. Boys, M. J. Miles. "Empirical Thermal Model for Inverter-Driver Cage Induction Machines" *IEE Proc. Electr. Power Appl.*, Vol. 141, No. 6, November 1994.

[6] NBR 5383. *Brazilian Induction Motor Standard*, Nov. 1982.

[7] D. S. Zhu, G. Champenois and C. Gruszczynski. "Coupling of Electrical and Thermal Models of an Induction Motor for Performance Prediction" *Proc. Int. Conf. on Electrical Machines, ICEM'90*, Mass., USA, 1990, pp.281-286.

[8] Mellor, P. H., Roberts, P., and Turner, D. R.. "Lumped Parameter Thermal Model for Electrical Machines of TEFC Design" *IEE Proc. B*, 1991, 138, 15, pp. 205-218.

[9] Neto, L.M., Salerno, C.H., Alvarenga, B.P.. "Harmonic Inductance in the Linear Analysis of Induction Motor" *International Conference on Electrical Machines in Australia - Adelaide*, Sep/1993.

[10] A. H. Eltom, N. S. Moharari. "Motor Temperature Estimation Incorporating Dynamic Rotor Impedance" *IEEE Trans. On Energy Conversion*, Vol. 6, No.1, March 1991.

[11] E. F. Fuchs, D. J. Roesler, K. P. Kovacs. "Aging of Electrical Appliances Due to Harmonics of the Power Systems Voltage" *IEEE Trans. On Power Delivery*, Vol. PWRD-1, No.3, July 1986.

[12] R. R. Dixon. "Thermal Aging Prediction from an Anhenius Plot with Only One Data Point" *IEEE Trans. Electrical Insulation*, Vol. EI-15, No. 4, 1980, pp. 331-334.

[13] Ruppert Filho, E., Arango, H., De Sá, J. S. "Analysis of Squirrel Cage Induction Motor Rotor Bars Thermal Behavior" *Proc. of International Conference on Electrical Machines*, pp. 245-250, Massachusetts, USA, 1990.

[14] M. Akbaba and S. Q. Fakhro. "New Model for Single-Unit Representation of Induction Motor Loads, Including Skin Effect, for Power System Transient Stability Studies" *IEE Proceedings-B,* vol. 6, no. 139, November 1992.

[15] Kostenko, M. aand Piotrovsky, L. *Electrical Machines*, MIR Publishers, Moscow, Russia, 1969.

A METHOD FOR CHARACTERIZATION OF THREE-PHASE UNBALANCED DIPS FROM RECORDED VOLTAGE WAVESHAPES

M.H.J. Bollen, L.D. Zhang
Dept. Electric Power Engineering
Chalmers University of Technology
Gothenburg, Sweden

Abstract: A proposal is presented for characterization of voltage dips as experienced by three-phase load. The authors propose this method for inclusion in international standards and recommendations. The method is based on the well-proven theory of symmetrical components. The primary result of the method is a so-called "characteristic magnitude" which corresponds to the magnitude (remaining voltage) as used for the existing methods to characterize dips experienced by single-phase load. Adding additional parameters where further accuracy is needed for characterization may extend the proposed method. For three-phase balanced dips the proposed method corresponds to the methods currently in use and recommended by international standards.

Introduction

All existing standard documents on voltage dips (sags) characterize a dip through one magnitude (remaining voltage or voltage drop) and one value for the duration [6,7,8]. There are obvious limitations to this method as one e.g. neglects the phase-angle jump [1] and the post-fault dip [2]. For the majority of sensitive single-phase equipment, the existing characterization enables a prediction of the behavior of the equipment during and after the event. Further, using a complex dip voltage can incorporate the phase-angle jump; giving the magnitude as a function of time can incorporate the post-fault dip.

Three-phase equipment will typically experience three different magnitudes, as the majority of dips are due to single-phase or phase-to-phase faults. The existing method of characterization uses the lowest of the three voltages and the longest duration. An example of a three-phase unbalanced dip is shown in Figure 1.

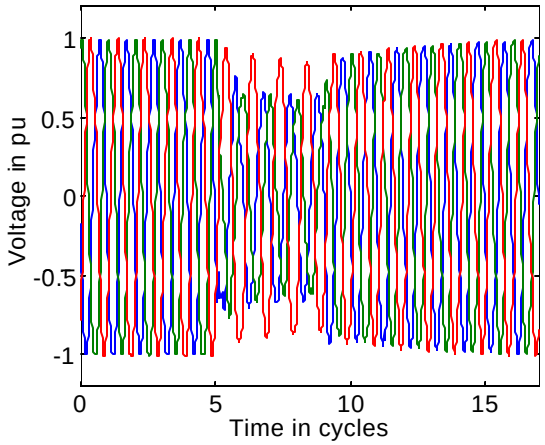

Figure 1: Example of a Three-Phase Unbalanced Dip

Dip characterization is often part of the voltage characteristics / power quality in general. In that case, the results should be applicable both to single-phase and three-phase equipment. Using the lowest of the three voltages to characterize the dip will result in erroneous results for both single-phase and three-phase equipment. An alternative technique is proposed in this document, which enables a characterization through one complex voltage, without significant loss of information. The method is based on the decomposition of the voltage phasors in symmetrical components.

An additional characteristic is introduced to enable exact reconstruction of the three complex voltages. The mathematics behind the method and additional examples are described in [3,4,5,9,10,11].

Background

Basic Classification

A classification of three-phase unbalanced dips was proposed in [5]. The classification considers three-phase, single-phase and phase-to-phase faults, star and delta-connected equipment and all types of transformer connection. It was further assumed that positive and negative-sequence source impedances are equal. This resulted in four types of three-phase unbalanced sag, shown as a phasor diagram in Figure 2. Type A is due to three-phase faults, types B, C and D are due to single-phase and phase-to-phase faults. Type B contains a zero-sequence component that is rarely transferred down to the equipment terminals. Three-phase equipment is normally connected in delta or in star without neutral connection. Single-phase low-voltage equipment is connected between phase and neutral, but the number of dips originating in the low-voltage system is small. Therefore the vast majority of three-phase unbalanced dips at the equipment terminals are of type C or type D, so that a distinction between type C and D is sufficient, together with a characteristic magnitude and phase-angle jump. The definition of characteristic magnitude and phase-angle jump is such that these do not change when the sag transfers from one voltage level to the other. The characteristic magnitude and phase-angle jump are defined as the absolute value and the argument of the complex phasor representing the voltage in the lowest phase for a type D dip, and the voltage between the two lowest phases for a type C dip.

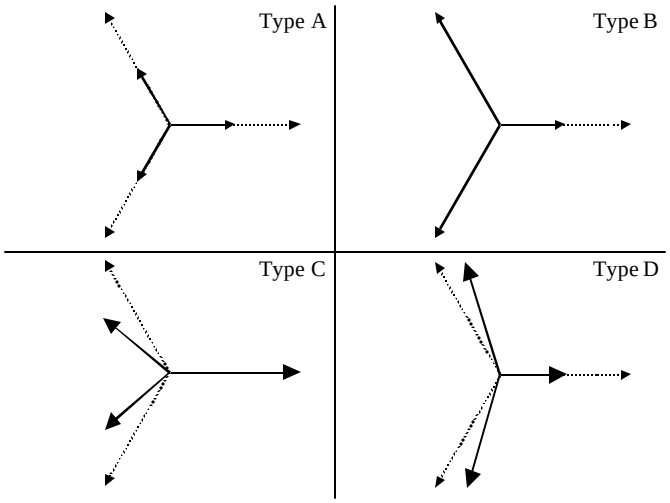

Figure 2: Four Types of Three-Phase Unbalanced Voltage Dips in Phasor- Diagram Form

The complex voltages for a three-phase unbalanced dip of type C with characteristic voltage $\overline{V}$ are as follows:

$$\begin{aligned}\overline{V}_a &= 1\\ \overline{V}_b &= -\tfrac{1}{2} - \tfrac{1}{2} j\overline{V}\sqrt{3}\\ \overline{V}_c &= -\tfrac{1}{2} + \tfrac{1}{2} j\overline{V}\sqrt{3}\end{aligned} \qquad (1)$$

For a dip of type D the complex voltages are:

$$\begin{aligned}\overline{V}_a &= 1\\ \overline{V}_b &= -\tfrac{1}{2}\overline{V} - \tfrac{1}{2} j\sqrt{3}\\ \overline{V}_c &= -\tfrac{1}{2}\overline{V} + \tfrac{1}{2} j\sqrt{3}\end{aligned} \qquad (2)$$

Generalization

A sound mathematical basis for the above classification is given in [3,4,10], including a generalization that holds when positive and negative-sequence source impedances are different. This extension of the classification is based on the theory of symmetrical components. The three (complex) phase voltages in an unbalanced three-phase system can be completely described through three component voltages, known as symmetrical components. Positive-sequence voltage $\overline{V}_1$, negative-sequence voltage $\overline{V}_2$ and zero-sequence voltage $\overline{V}_0$ are calculated from the complex phase voltages $\overline{V}_a$, $\overline{V}_b$ and $\overline{V}_c$ as follows:

$$\begin{bmatrix}\overline{V}_0\\ \overline{V}_1\\ \overline{V}_2\end{bmatrix} = \frac{1}{3}\begin{bmatrix}1 & 1 & 1\\ 1 & a & a^2\\ 1 & a^2 & a\end{bmatrix}\begin{bmatrix}\overline{V}_a\\ \overline{V}_b\\ \overline{V}_c\end{bmatrix} \qquad (3)$$

where

$a = -\tfrac{1}{2} + \tfrac{1}{2} j\sqrt{3}$.

Knowing the complex sequence voltages, the voltages in the three phases can be calculated from:

$$\begin{bmatrix}\overline{V}_a\\ \overline{V}_b\\ \overline{V}_c\end{bmatrix} = \begin{bmatrix}1 & 1 & 0\\ 1 & -\tfrac{1}{2} & -\tfrac{1}{2} j\sqrt{3}\\ 1 & -\tfrac{1}{2} & \tfrac{1}{2} j\sqrt{3}\end{bmatrix}\begin{bmatrix}\overline{V}_0\\ \overline{V}_1 + \overline{V}_2\\ \overline{V}_1 - \overline{V}_2\end{bmatrix} \qquad (4)$$

Comparing (4) with (1) and (2), shows that the following relations hold for a dip of type C:

$$\begin{aligned}\overline{V}_0 &= 0\\ \overline{V}_1 + \overline{V}_2 &= 1\\ \overline{V}_1 - \overline{V}_2 &= \overline{V}\end{aligned} \qquad (5)$$

The equivalent expressions for a dip of type D are:

$$\begin{aligned} \overline{V}_0 &= 0 \\ \overline{V}_1 + \overline{V}_2 &= \overline{V} \\ \overline{V}_1 - \overline{V}_2 &= 1 \end{aligned} \qquad (6)$$

In the proposed characterization method these relations are used to obtain the characteristic complex voltage $\overline{V}$. The underlying assumption for (5) and (6) is that positive and negative-sequence source impedances are identical. As this is not exactly the case in reality, a second dip characteristic is introduced: the PN-factor $\overline{F}$. For a dip of type C the definitions are as follows:

$$\begin{aligned} \overline{V} &= \overline{V}_1 - \overline{V}_2 \\ \overline{F} &= \overline{V}_1 + \overline{V}_2 \end{aligned} \qquad (7)$$

For a dip of type D the definitions are as follows:

$$\begin{aligned} \overline{V} &= \overline{V}_1 + \overline{V}_2 \\ \overline{F} &= \overline{V}_1 - \overline{V}_2 \end{aligned} \qquad (8)$$

A method to obtain the type of dip from the recorded voltages will be discussed below.

Symmetrical Phase

Expression (4) gives the symmetrical components with reference to phase a. Expressions (1) and (2) are valid for a fault in phase a or between phases b and c, i.e. with phase a as the symmetrical phase. Including all three possible symmetrical phases results in six (sub) types of three-phase unbalanced dips: C_a, C_b, C_c and D_a, D_b, D_c. Expression (1) describes a dip of type Ca; expression (2) describes a dip of type D_a. Expressions for the complex voltages of the all six types are given in Table 1. It has been assumed that in all cases, the positive real axis is along the a-phase pre-event voltage.

For phasor diagrams as shown in Figure 2, the selection of the symmetrical phase is straightforward: the lowest phase for type D, the highest phase for type C. For a non-unity PN-factor and a non-zero phase- angle jump, it may become less obvious which phase is the symmetrical phase. The method proposed in [3,4] transforms phase voltage to symmetrical components to obtain the symmetrical phase.

Transforming the 6 different three-phase unbalanced dips to symmetrical components, by using (3), results in the expressions for positive-sequence voltage V_1 and negative-sequence voltage V_2 summarized in Table 2. Note that in all cases the positive real axis is along the a-phase pre- event voltage and in all cases expression (3) has been used to obtain the positive and negative-sequence voltages (i.e. the symmetrical component transformation with phase a as reference phase).

From Table 2 it follows that the positive-sequence voltage is type independent. The direction of the positive-sequence voltage is along the reference axis (phase a pre-event voltage in this case) if the argument of the characteristic complex voltage is neglected. The direction of the negative-sequence voltage depends on the type of dip. By rotating the negative-sequence voltage over an integer multiple of 60º all dip types can be obtained from one prototype dip. Dip type C_a has

been chosen as prototype dip. From Table 2, the following relation between positive and negative sequence voltage is obtained for the prototype dip:

$$\overline{V}_{2,ref} = 1 - \overline{V}_1 \qquad (9)$$

Table 1: Complex Voltages for Three-Phase Unbalanced Dips

Type C_a	Type C_b
$\overline{V}_a = 1$ $\overline{V}_b = -\frac{1}{2} - \frac{1}{2} j\overline{V}\sqrt{3}$ $\overline{V}_c = -\frac{1}{2} + \frac{1}{2} j\overline{V}\sqrt{3}$	$\overline{V}_a = 1$ $\overline{V}_b = -\frac{1}{2}\overline{V} - \frac{1}{2} j\sqrt{3}$ $\overline{V}_c = -\frac{1}{2}\overline{V} + \frac{1}{2} j\sqrt{3}$
Type C_b	Type D_b
$\overline{V}_a = \frac{1}{4} + \frac{3}{4}\overline{V} + \frac{1}{4} j\sqrt{3} - \frac{1}{4} j\overline{V}\sqrt{3}$ $\overline{V}_b = -\frac{1}{2} - \frac{1}{2} j\sqrt{3}$ $\overline{V}_c = \frac{1}{4} - \frac{3}{4}\overline{V} + \frac{1}{4} j\sqrt{3} + \frac{1}{4} j\overline{V}\sqrt{3}$	$\overline{V}_a = \frac{1}{4}\overline{V} + \frac{3}{4} - \frac{1}{4} j\sqrt{3} + \frac{1}{4} j\overline{V}\sqrt{3}$ $\overline{V}_b = -\frac{1}{2}\overline{V} - \frac{1}{2} j\overline{V}\sqrt{3}$ $\overline{V}_c = \frac{1}{4}\overline{V} - \frac{3}{4} + \frac{1}{4} j\sqrt{3} + \frac{1}{4} j\overline{V}\sqrt{3}$
Type C_c	Type D_c
$\overline{V}_a = \frac{1}{4} + \frac{3}{4}\overline{V} - \frac{1}{4} j\sqrt{3} + \frac{1}{4} j\overline{V}\sqrt{3}$ $\overline{V}_b = \frac{1}{4} - \frac{3}{4}\overline{V} - \frac{1}{4} j\sqrt{3} - \frac{1}{4} j\overline{V}\sqrt{3}$ $\overline{V}_c - \frac{1}{2} + \frac{1}{2} j\sqrt{3}$	$\overline{V}_a = \frac{1}{4}\overline{V} + \frac{3}{4} + \frac{1}{4} j\sqrt{3} - \frac{1}{4} j\overline{V}\sqrt{3}$ $\overline{V}_b = \frac{1}{4}\overline{V} - \frac{3}{4} - \frac{1}{4} j\sqrt{3} - \frac{1}{4} j\overline{V}\sqrt{3}$ $\overline{V}_c - \frac{1}{2}\overline{V} + \frac{1}{2} j\overline{V}\sqrt{3}$

Table 2: Symmetrical Components for Three-Phase Unbalanced Dips

Type C_a	**Type D_a**
$\overline{V}_1 = \frac{1+\overline{V}}{2}$ $\overline{V}_2 = \frac{1-\overline{V}}{2}$	$\overline{V}_1 = \frac{1+\overline{V}}{2}$ $\overline{V}_2 = -\frac{1-\overline{V}}{2}$
Type C_b	**Type D_b**
$\overline{V}_1 = \frac{1+\overline{V}}{2}$ $\overline{V}_2 = a \bullet \frac{1-\overline{V}}{2}$	$\overline{V}_1 = \frac{1+\overline{V}}{2}$ $\overline{V}_2 = -a \bullet \frac{1-\overline{V}}{2}$
Type C_c	**Type D_c**
$\overline{V}_1 = \frac{1+\overline{V}}{2}$ $\overline{V}_2 = a^2 \bullet \frac{1-\overline{V}}{2}$	$\overline{V}_1 = \frac{1+\overline{V}}{2}$ $\overline{V}_2 = -a^2 \bullet \frac{1-\overline{V}}{2}$

The dip type may be obtained from the angle between the negative-sequence voltage of the measured dip and the negative-sequence voltage of the prototype dip. Due to various approximations made and measurement errors, this angle is not exactly an integer multiple of 60º so that the following expression may be used to obtain the dip type:

$$k = \text{round}\left(\frac{\text{angle}\left(\overline{V}_2, 1-\overline{V}_1\right)}{60^{\,o}}\right) \tag{10}$$

k=0: type Ca
k=1: type Dc
k=2: type Cb
k=3: type Da
k=4: type Cc
k=5: type Db

Knowing the dip type, the negative-sequence voltage can be calculated back to the corresponding value for the prototype dip:

$$\overline{V}_2' = \overline{V}_2 e^{-jk60^o} \tag{11}$$

where k is obtained according to (10) and the negative sequence voltage of the measured dip. Characteristic voltage $\overline{V}$ and PN-factor $\overline{F}$ are obtained from the expressions for the prototype dip (7):

$$\begin{aligned} \overline{V} &= \overline{V}_1 - \overline{V}_2' \\ \overline{F} &= \overline{V}_1 + \overline{V}_2' \end{aligned} \tag{12}$$

Overview of Characterization

This method has been applied to recorded dips in both transmission (220 and 400 kV) and distribution (11 and 33 kV) systems. It was shown that the PN-factor is very close to unity in transmission systems. In distribution systems, the PN-factor is typically less than unity due to the effect of induction motor load. But even in distribution systems, the PN-factor is rarely less than 90% in absolute value [10].

The result is that the characteristic magnitude (the absolute value of the characteristic complex voltage $\overline{V}$) can be used to characterize three-phase unbalanced dips without loss of essential information. Using characteristic magnitude and duration for three-phase unbalanced dips, corresponds to the existing classification (through magnitude and duration) for single-phase equipment. Where needed, the characterization for three-phase unbalanced dips may be extended in several ways:

- Characteristic phase-angle jump may be defined as the argument of the complex characteristic voltage in the same way as the phase-angle jump may be used as an additional characteristic for dips experienced by single-phase equipment.
- PN-factor may be used as an additional characteristic in case positive and negative-sequence source impedances differ significantly. This is the case in systems with a large amount of induction motor load.

- Zero-sequence voltage is needed as an additional characteristic for specific system configurations in combination with three-phase star-connected load.
- Characteristic magnitude, characteristic phase-angle jump and PN-factor may all be given as a function of time.

The Proposed Method

The proposal is to use characteristic complex voltage and PN-factor to characterize three-phase unbalanced dips. The proposed algorithm for classification and characterizatio n consists of a number of steps. It is assumed that time-domain sampled data is available for the three phases including at least two cycles pre-event voltages.

I. Determine the voltage frequency from the pre-event voltage samples.
II. Determine voltage phasors for the three phase voltages by using a DFT (Discrete Fourier Transform) algorithm. The voltage frequency is used to obtain the phase shift between the during-event and the pre-event voltages.
III. Obtain positive, negative and zero-sequence voltages by using expression (3).
IV. Determine if the dip is balanced or unbalanced from the magnitude of the negative sequence voltage compared to the positive sequence voltage.
V. For balanced dips the dip type is A and the characteristic voltage equals the positive sequence voltage.
VI. For unbalanced dips the dip type is determined from positive and negative-sequence voltages by using expression (10), characteristic voltage and PN-factor are obtained by using expression (12).
VII. A balanced dip is fully characterized through the characteristic voltage.
VIII. An unbalanced dip is fully characterized through dip type, characteristic voltage, PN-factor and zero-sequence voltage.
IX. The characteristic magnitude is obtained as the absolute value of the characteristic voltage. The phase-angle jump is obtained as the argument of the characteristic voltage.

Example of Characterization

The above-proposed method has been applied to the three-phase unbalanced dip shown in Figure 1. The rms voltage as a function of time, for the three voltages, is shown in Figure 3.

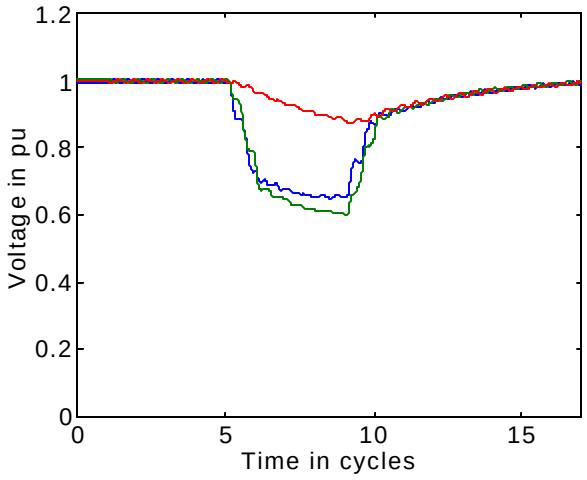

Figure 3: RMS Voltage Versus Time for the Three Voltages in Figure 1

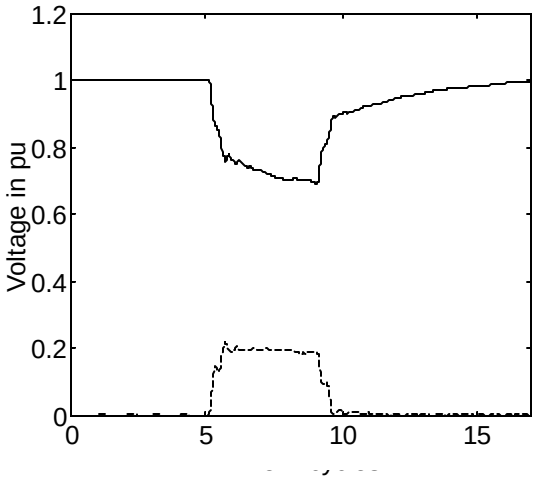

Figure 4: Positive-Sequence Voltage (Solid Curve) and Negative-Sequence Voltage (Dashed Curve) for the Dip in Figure 1

Figure 4 shows positive and negative-sequence voltage, obtained by using expression (3). Fault initiation takes places about 5 cycles after the start of the recording. Fault clearing is 4.5 cycles later. Before fault initiation and after fault clearing, the negative-sequence voltage is small, in other words: the voltages are balanced. Note that the positive-sequence voltage does not immediately recover upon fault clearing. This is probably due to induction motor load taking a larger current when their speed has dropped below nominal speed.

Figure 5 plots the angle in the complex plane between the negative-sequence voltage and the drop in positive-sequence voltage, as used in (10). When the negative-sequence voltage is less than 0.02 pu, the angle is given a small negative value. This same threshold is also used to distinguish between a balanced and an unbalanced dip.

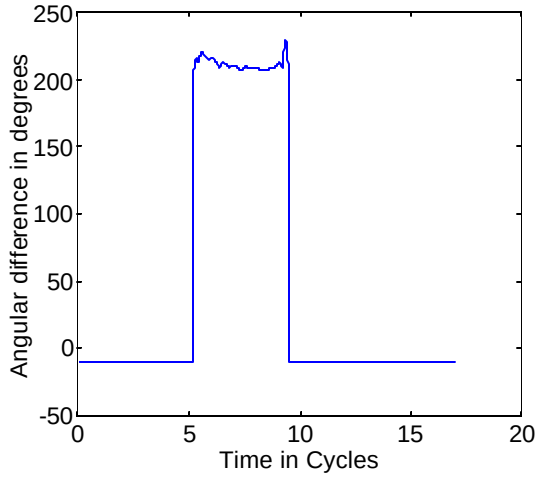

Figure 5: Angle Between (Complex) Negative-Sequence Voltage and (Complex) Drop in Positive-Sequence Voltage, for the Dip in Figure 1

From the angular difference in Figure 5, the dip type is determined by using (10). The result is shown in Figure 6. The integer value of the dip type is according to the list below (10), where dip type 6 is a balanced dip (Type A). Note that also before the fault, the event is characterized as type A. This is due to the criterion used to detect a type A dip: negative-sequence voltage less than 0.02 pu. Therefore the normal supply is characterized as a type A dip without voltage drop (100% characteristic magnitude). From Figure 6 it can be concluded that the dip shown in Figure 1 is of type C_C: a drop in phases a and b with no drop or a minor drop in phase c. This is exactly as shown in Figure 1, but would be hard for an automatic algorithm to detect. Also will it not in all cases be straightforward which is the type of a three-phase unbalanced dip. Around fault initiation and around fault clearing the algorithm indicates a different dip type. This is due to the method used to obtain the complex phase voltages, which takes about one cycle for the transition. During such a transition especially the angle of the complex voltage may obtain unrealistic values. Increasing the negative-sequence value below which the dip is classified as balanced may solve the problem. Other methods may need to be developed for this.

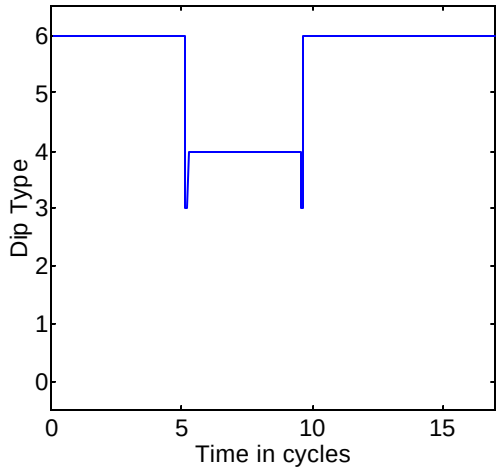

Figure 6: Dip Type Versus Time for the Dip in Figure 1

The positive and negative-sequence voltages, together with the dip type, give the characteristic voltage and the PN-factor for the dip. The result is shown in Figure 7. Before fault initiation and after fault clearing, characteristic magnitude and PN-factor are almost equal because the negative-sequence voltage is very small. During the fault, both characteristic voltage and PN-factor show a decreasing trend. The PN-factor is continuous, i.e. it does not show a jump at fault initiation or at fault clearing. This behavior may be explained from the deceleration of induction motor load during the fault and their acceleration after the fault. The lower the motor speed, the lower their impedance and the more the voltage in the system is reduced. The PN factor is thus an indication of the effect of the load on the voltage dip. This relation, and the underlying mathematical models, is described in detail in [10].

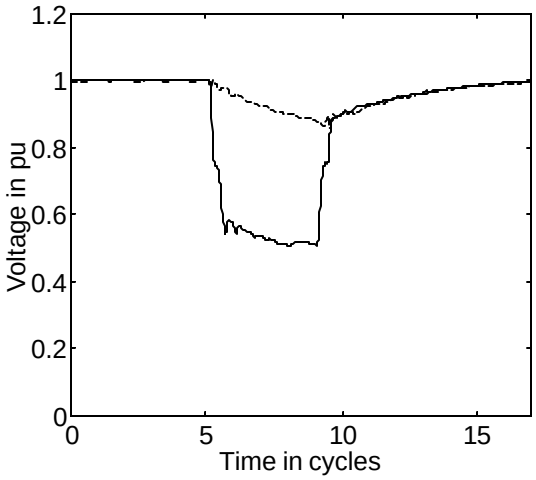

Figure 7: Characteristic Voltage (Solid Line) and PN-Factor (Dashed Line) for the Dip in Figure 1

Conclusion

A new method has been proposed for characterization of three-phase unbalanced voltage dips. The result of the characterization is a simple characteristic magnitude. This single value enables a prediction of the effect of the event on most single-phase and three-phase equipment. When more detailed characterization of the event is required, additional parameters can be added. For three-phase balanced dips, the proposed characterization corresponds to the methods currently in use and recommended by international standards [6,7,8].

References

[1] M.H.J.Bollen, P. Wang, N. Jenkins, Analysis and consequences of the phase jump associated with a voltage sag, Power System Computation Conference, Dresden, Germany, August 1996.

[2] M.H.J. Bollen, The influence of motor re-acceleration on voltage sags, IEEE Transactions on Industry Applications, vol.31, 1995, p.667-674.

[3] L.D. Zhang, M.H.J. Bollen, A method for characterizing unbalanced voltage dips (sags) with symmetrical components, IEEE Power Engineering Letters, July 1998.

[4] L.D. Zhang, M.H.J. Bollen, Characteristics of voltage dips (sags) in power systems, IEEE Transactions on Power Delivery, in print.

[5] M.H.J. Bollen, Characterization of voltage sags experienced by three-phase adjustable-speed drives, IEEE Transactions on Power Delivery, Vol.12, no.4, October 1997, pp.1666-1671.

[6] Electromagnetic Compatibility (EMC), Part 4. Testing and measurement protocols. Section 11. Voltage dips, short interruptions and voltage variations immunity tests. IEC document 61000-4-11.

[7] Recommended practice for evaluating electric power system compatibility with electronic process equipment, IEEE Std. 1346-1998.

[8] Measurement guide for voltage characteristics, UNIPEDE report 23002 Ren 9531.

[9] M.H.J. Bollen, Understanding power quality problems - voltage sags and interruptions, IEEE Press, 1999.

[10] L. Zhang, Three-phase unbalance of voltage dips, Licentiate thesis, Chalmers University of Technology, Dept Electric Power Engineering, Gothenburg, Sweden, November 1999.

[11] M.H.J. Bollen, L.D. Zhang, Analysis of voltage tolerance of ac adjustable-speed drives for three-phase balanced and unbalanced sags, IEEE Transactions on Industry Applications, in print.